Leaky severe combined immunodeficiency in mice lacking non-homologous end joining factors XLF and Mri

Sergio Castañeda-Zegarra[1,2,†], Qindong Zhang[1,2,†], Amin Alirezaylavasani[1,2], Valentyn Oksenych[1,2,3]*

[1]Department of Clinical and Molecular Medicine (IKOM), Norwegian University of Science and technology, 7491 Trondheim, Norway;

[2]St. Olavs Hospital, Trondheim University Hospital, Clinic of Medicine, Postboks 3250 Sluppen, 7006 Trondheim;

[3]Department of Biosciences and Nutrition (BioNut), Karolinska Institutet, 14183 Huddinge, Sweden

[†]These authors contributed equally

*Correspondence: valentyn.oksenych@ntnu.no;

Keywords: NHEJ; Cernunnos; Cyren; pro-B cells; lymphocyte; genetic interaction

Abstract

Non-homologous end joining (NHEJ) is a DNA repair pathway required to detect, process and ligate DNA double-stranded breaks (DSBs) throughout the cell cycle. The NHEJ pathway is required for the V(D)J recombination in developing B and T lymphocytes. During the NHEJ, the core factors Ku70 and Ku80 form a heterodimer called Ku, which recognizes DSBs and promotes the recruitment of accessory factors (e.g., PAXX, Mri, Dna-pkcs, Artemis) and downstream core factors XLF, XRCC4, and Lig4. Mutations in NHEJ genes result in immunodeficiency. Deletion of individual NHEJ genes *Mri, Paxx* or *Xlf* in mice resulted in no or modest phenotype, while combined inactivation of *Xlf* and *Mri,* or *Xlf* and *Paxx,* led to late embryonic lethality. Here, we demonstrated that the deletion of pro-apoptotic factor *Trp53* rescued the embryonic lethality of mice with combined deficiencies in *Xlf* and *Mri*. The $Xlf^{-/-}Mri^{-/-}Trp53^{+/-}$ mice possessed reduced body weight, severely reduced B and T cell lymphocyte counts in spleen and thymus, and accumulation of progenitor B cells in the bone marrow. To the contrary, combined inactivation of *Mri* and *Paxx* resulted in live-born mice with phenotype not distinguishable from Mri-deficient mice. We concluded that Mri is functionally redundant with XLF during the B and T lymphocyte development *in vivo*.

1. Introduction

The non-homologous end-joining (NHEJ) is the DNA repair pathway that recognizes, processes and ligates DNA double-stranded breaks (DSB) throughout the cell cycle. The NHEJ is required for lymphocyte development, in particular, to repair DSBs induced by the recombination activating genes 1 and 2 (RAG) in developing B and T lymphocytes, and by activation-induced cytidine deaminase (AID) in mature B cells [1]. The NHEJ is initiated when core subunits Ku70 and Ku80 (Ku) are recruited to the DSB sites. Ku then mediates the recruitment of accessory NHEJ factors, including the DNA-dependent protein kinase catalytic subunit (DNA-PKcs) and nuclease Artemis. Additional core factors DNA ligase 4 (Lig4), X-ray repair cross-complementing protein 4 (XRCC4) and XRCC4-like factor (XLF) mediate DNA end ligation. Accessory factors paralogue of XRCC4 and XLF (PAXX) and modulator of retroviral infection (Mri) stabilize the NHEJ complex [2, 3]. Inactivation of *Ku70*, *Ku80*, *Dna-pkcs* or *Artemis* results in severe combined immunodeficiency (SCID) characterized by a lack of mature B and T lymphocytes [4-8]. Deletion of *Xrcc4* [9] or *Lig4* [10] results in late embryonic lethality in mice that correlates with apoptosis in the central nervous system. Inactivation of the *Xlf* (*Cernunnos*) gene results in only modest immunodeficiency in mice [11, 12], while mice lacking *Paxx* [13-16] or *Mri* [2, 17] displayed no overt immunodeficiency phenotype.

Mild phenotype observed in mice lacking XLF was explained by functional redundancy between XLF and multiple DNA repair factors, including *Ataxia telangiectasia* mutated (ATM), histone H2AX [18], Mediator of DNA Damage Checkpoint 1 (MDC1) [19], p53-binding protein 1 (53BP1) [16, 20], RAG2 [21], DNA-PKcs [19, 22, 23], PAXX [3, 13, 14, 19, 24-26] and Mri [2]. Moreover, combined inactivation of *Xlf* and *Paxx*, as well as *Xlf* and *Mri*, resulted in late embryonic lethality in mice, which challenged studies of B and T lymphocyte development *in vivo*.

In this study, we rescued synthetic lethality between *Xlf* and *Mri* by inactivating one or two alleles of pro-apoptotic gene *Trp53*. Resulting *Xlf*$^{-/-}$*Mri*$^{-/-}$*Trp53*$^{+/-}$ mice possessed leaky SCID phenotype with nearly no B and T lymphocytes detected in spleens, nearly no mature T cells detected in thymi, and

accumulated progenitor B cells in the bone marrow. The *Xlf*$^{-/-}$*Paxx*$^{-/-}$*Trp53*$^{+/-}$ mice possessed a more severe phenotype with even lower levels of mature B cells detected in the spleen. Therefore, we concluded that both PAXX and Mri function in B and T lymphocyte development *in vivo*, and their roles are compensated by XLF.

2. Materials and Methods

2.1. Mice

All experiments involving mice were performed according to the protocols approved by the Comparative Medicine Core Facility (CoMed) at the Norwegian University of Science and Technology (NTNU, Trondheim, Norway). *Xlf*$^{+/-}$ [11] and *Dna-pkcs*$^{+/-}$ [4] mice were imported from the laboratory of Professor Frederick W. Alt at Harvard Medical School. *Trp53*$^{+/-}$ mice [27] were imported from Jackson Laboratories. *Paxx*$^{+/-}$ [15] and *Mri*$^{+/-}$ [17] mice were generated on request for the Oksenych group and described previously.

2.2. Lymphocyte development

Lymphocyte populations were analyzed by flow cytometry as described earlier [15, 17, 18, 20]. Briefly, spleens, thymi, and femora were isolated from 5-7-week-old mice, the cells were lysed using red blood cell lysis buffer Hybri-Max™ (Sigma Aldrich, St. Louis, MO, USA; #R7757), resuspended either in PBS (Thermo Scientific, Basingstoke, UK; #BR0014G) or in 95% PBS-5% Fetal bovine serum, FCS (Sigma Life Science, St. Louis, Missouri, United States; Cat#F7524), and counted using Countess™ II Automated Cell Counter (Invitrogen, Carlsbad, CA, United States; #A27977). The cell suspension was spun down and diluted with PBS to get a final cell concentration of 2.5 x 10^7/mL. The cells were then incubated with fluorochrome-conjugated antibodies and analyzed by flow cytometry.

2.3. Antibodies

For the flow cytometry analyses, the following antibodies were used: rat anti-CD4-PE-Cy7 (BD Pharmingen™, Binningerstrasse, Allschwil, Switzerland, #552775, 1:100); rat anti-CD8-PE-Cy5 (BD Pharmingen™, Binningerstrasse, Allschwil, Switzerland, #553034, 1:100); anti-CD19-PE-Cy7 (Biolegend, San Diego, CA, USA, #115520, 1:100); hamster anti-mouse anti-CD3-FITC (BD Pharmingen™, Binningerstrasse, Allschwil, Switzerland, #561827, 1:100); rat anti-mouse anti-CD43-FITC (BD Pharmingen™, Binningerstrasse, Allschwil, Switzerland, #561856, 1:100); rat anti-mouse anti-CD45R/B220-APC (BD Pharmingen™, Binningerstrasse, Allschwil, Switzerland; #553092, 1:100); rat anti-mouse anti-IgM-PE-Cy7 (BD Pharmingen™, Binningerstrasse, Allschwil, Switzerland, #552867, 1:100).

2.4. Statistics

Statistical analyses were performed using one-way ANOVA, GraphPad Prism 8.0.1. 244 (San Diego, CA, USA). In all statistical tests, $p<0.05$ were taken to be significant (*, $p<0.05$; **, $p<0.01$; ***, $p<0.001$; ****, $p<0.0001$).

3. Results

3.1. Inactivation of the Trp53 gene rescued embryonic lethality in mice lacking XLF and Mri

Combined inactivation of *Xlf* and *Mri* resulted in synthetic lethality [2]. To rescue embryonic lethality in *Xlf*$^{-/-}$*Mri*$^{-/-}$ mice, we inactivated one allele of *Trp53*. For this, we intercrossed *Mri*$^{-/-}$ [17] and *Xlf*$^{-/-}$*Trp53*$^{+/-}$ [19] mice. In the next step, we selected and intercrossed triple heterozygous mice, *Xlf*$^{+/-}$*Mri*$^{+/-}$*Trp53*$^{+/-}$. By PCR screening, we identified *Xlf*$^{-/-}$*Mri*$^{-/-}$*Trp53*$^{+/-}$ (n=6), *Xlf*$^{-/-}$*Mri*$^{-/-}$*Trp53*$^{-/-}$ (n=2) and one *Xlf*$^{-/-}$*Mri*$^{-/-}$ mice (Fig. 1). The mice lacking both XLF and Mri factors possessed reduced weight (12 g on average, p<0.0001) when compared with gender- and age-matched WT (19 g), *Xlf*$^{-/-}$ (19 g) and *Mri*$^{-/-}$ (20 g) controls. We used these mice to characterize the development of B and T lymphocytes (Fig. 1-4).

3.2. Leaky SCID in $Xlf^{-/-}Mri^{-/-}Trp53^{+/-}$ mice

To determine the roles of Mri in lymphocyte development *in vivo*, we isolated thymi, spleens and femora from $Xlf^{-/-}Mri^{-/-}Trp53^{+/-}$ mice, as well as from the $Xlf^{-/-}$, $Mri^{-/-}$ and WT controls. Combined deficiency for XLF and Mri resulted in 3-fold reduced sizes of thymi (32 mg, on average, $p<0.0001$) and 9-fold reduced counts of thymocytes ($1.9x10^7$, $p<0.0001$), when compared with single deficient or WT controls (Fig. 1). The average weight of spleens (22 mg, $p<0.0001$), as well as a count of splenocytes ($2x10^7$, $p<0.0001$) were about 4-5-fold reduced in 6-week-old $Xlf^{-/-}Mri^{-/-}Trp53^{+/-}$ mice when compared with WT and single deficient controls (Fig. 1). The reduced number of splenocytes was due to decreased populations of B and T lymphocytes (Fig. 2). In particular, the reduction of CD3+ T cells count was 4 folds ($p<0.0001$), while the count of CD19+ B cells was 20 folds reduced ($p<0.0001$) in $Xlf^{-/-}Mri^{-/-}Trp53^{+/-}$ mice when compared with single deficient and WT controls (Fig. 2). Counts of all CD4+, CD8+ and CD4+CD8+ T cells in thymi, as well as counts of CD4+ and CD8+ T cells in spleens, were dramatically reduced in $Xlf^{-/-}Mri^{-/-}Trp53^{+/-}$ mice when compared with single deficient and wild type controls (about 4 folds, $p<0.0001$; Fig. 2). We concluded that XLF and Mri are functionally redundant during the B and T lymphocytes development in mice.

3.3. Leaky SCID in mice lacking XLF and PAXX

Combined inactivation of XLF and PAXX resulted in embryonic lethality in mice [3, 13, 14, 19]. To determine the impact of XLF and PAXX on B and T cell development *in vivo*, we rescued the synthetic lethality by inactivating one allele of *Trp53* as described earlier [19]. Resulting $Xlf^{-/-}Paxx^{-/-}Trp53^{+/-}$ mice possessed 30-40 folds reduced counts of thymocytes ($4x10^6$, $p<0.0001$) when compared with WT ($1.31x10^8$), $Xlf^{-/-}$ ($1.36x10^8$) and $Paxx^{-/-}$ ($1.66x10^8$) mice (Fig. 2, 3) due to decreased levels of both double-positive CD4+CD8+ and single-positive CD4+ and CD8+ T cells (Fig. 2,3). Development of spleens in 6-week old mice lacking both XLF and PAXX was dramatically affected when compared with WT and single deficient controls due to the lack of B cells and decreased counts of T cells (Fig. 3). In particular, when compared with the WT and single knockout controls, in

Xlf$^{-/-}$*Paxx*$^{-/-}$*Trp53*$^{+/-}$ mice the counts of CD19+ B splenocytes were reduced 400-600 folds ($0.1x10^6$, $p<0.0001$); and the counts of CD3+ T splenocytes were reduced 70-90 folds (to $0.3x10^6$). We concluded that XLF and PAXX are functionally redundant during the B and T lymphocyte development in mice.

3.4. Early B cell development is abrogated in mice lacking XLF and Mri, or XLF and PAXX

Reduced counts and proportions of mature B lymphocytes in *Xlf*$^{-/-}$*Mri*$^{-/-}$*Trp53*$^{+/-}$ mice suggested a block in B cell development in the bone marrow. We isolated the bone marrow cells from the femora of mice lacking XLF, Mri or both XLF/Mri and analyzed proportions of B220+CD43+IgM- progenitor B cells, B220+CD43-IgM- pre-B cells and B220+CD43-IgM+ immature and mature B cells. We detected only background levels of B220+CD43-IgM+ B cells in bone marrows isolated from *Xlf*$^{-/-}$*Mri*$^{-/-}$*Trp53*$^{+/-}$ mice (Fig. 4A,B). To the contrary, these mice possessed 2-3 fold increased proportions of pro-B cells when compared with WT, *Mri*$^{-/-}$ and *Xlf*$^{-/-}$ controls (Fig. 4A, C). Moreover, *Xlf*$^{-/-}$*Paxx*$^{-/-}$*Trp53*$^{+/-}$ mice possessed background levels of IgM+ B cells, and 3-4 folds increased proportions of pro-B cells when compared with WT, *Paxx*$^{-/-}$ and *Xlf*$^{-/-}$ controls ($p<0.0001$; Fig. 4A,C). We concluded that B cell development is blocked at pro-B and pre-B cell stages of both *Xlf*$^{-/-}$*Mri*$^{-/-}$*Trp53*$^{+/-}$ and *Xlf*$^{-/-}$*Paxx*$^{-/-}$*Trp53*$^{+/-}$ mice.

3.5. Normal development of Paxx$^{-/-}$*Mri*$^{-/-}$ *mice*

Both PAXX and Mri are accessory NHEJ factors that are functionally redundant with XLF in mouse development. Combined inactivation of *Paxx* and *Xlf* [3, 13, 14, 19], or *Mri* and *Xlf* ([2]; this study) genes resulted in synthetic lethality in mice, as well as in abrogated V(D)J recombination in vAbl pre-B cells [2, 3, 13, 14, 25]. To determine if *Paxx* genetically interacts with *Mri*, we intercrossed mice heterozygous or null for both genes (e.g., *Paxx*$^{+/-}$*Mri*$^{+/-}$). We found that resulting *Paxx*$^{-/-}$*Mri*$^{-/-}$ double knockout mice are of nearly WT size (17 g, $p>0.9999$), fertile, and possess normal development of B and T cells, indistinguishable from wild type and single deficient *Paxx*$^{-/-}$ and *Mri*$^{-/-}$ controls. In particular, *Paxx*$^{-/-}$*Mri*$^{-/-}$ mice possessed normal counts of thymocytes and splenocytes,

including the CD4+, CD8+, and CD4+CD8+ T cells; and CD19+ B cells (not shown). We concluded that there is no genetic interaction between *Paxx* and *Mri* genes *in vivo*.

4. Discussion

Genetic inactivation of *Xlf* [11], *Paxx* [3, 13-15], or *Mri* [2, 28] in mice resulted in modest or no detectable phenotype. However, inactivation of other NHEJ factors resulted in the blockage of B and T cell development in mice, e.g., observed in *Ku70*$^{-/-}$ [5], *Ku80*$^{-/-}$ [6], *Artemis*$^{-/-}$ [7], *Dna-pkcs*$^{-/-}$ [4]; or embryonic lethality, e.g., *Xrcc4*$^{-/-}$ [9] and *Lig4*$^{-/-}$ [10]. Moreover, combined inactivation of *Xlf* and *Mri* (*Xlf*$^{-/-}$*Mri*$^{-/-}$) [2] or *Xlf* and *Paxx* (*Xlf*$^{-/-}$*Paxx*$^{-/-}$) [3, 13, 14], also resulted in embryonic lethality in mice, which correlated with increased levels of neuronal apoptosis in the central nervous system. Inactivation of one or two alleles of *Trp53* rescued the embryonic lethality of the *Xrcc4*$^{-/-}$[9, 29], *Lig4*$^{-/-}$[10, 30], *Xlf*$^{-/-}$*Dna-pkcs*$^{-/-}$ and *Xlf*$^{-/-}$*Paxx*$^{-/-}$[19; 23]. Findings during the last years suggest that Mri forms heterogeneous complexes containing PAXX or XLF, which function during DNA DSB repair by the NHEJ [2]. Combined inactivation of *Xlf* and *Mri* in vAbl pre-B cells resulted in a severe block in V(D)J recombination and accumulation of unrepaired DNA double-strand breaks *in vitro* [2]. However, it was unclear whether the combined inactivation of *Xlf* and *Mri* will result in the lack of B and T lymphocytes in adult mice. Similarly, the double deficient vAbl pre-B cells lacking *Xlf* and *Paxx* were unable to maintain the V(D)J recombination. However, it was not known whether the double-deficient mice lacking XLF and PAXX will possess any mature B cells. Importantly, the lack of progenitor T cell model system left the question on T cell development in *Xlf*$^{-/-}$*Mri*$^{-/-}$ and *Xlf*$^{-/-}$*Paxx*$^{-/-}$ mice completely unexplored.

Here, we demonstrated that mice lacking XLF, Mri and p53, although liveborn, possessed a leaky severe combined immunodeficiency phenotype. The *Xlf*$^{-/-}$*Mri*$^{-/-}$*Trp53*$^{+/-}$ mice, however, had a clear fraction of mature B cells in the spleen (CD19+) and bone marrow (B220+CD43-IgM+) (Fig. 2, 4), as well as clear fractions of double and single-positive T cells in the thymus (CD4+CD8+, CD4+, CD8+) and single-positive T cells in the spleen (CD4+ and CD8+) (Fig. 2). Similarly, the triple deficient mouse

model lacking XLF, PAXX, and p53 was liveborn and possessed only minor proportions of mature B cells in spleen and bone marrow, as well as only minor fractions of mature single positive T cells in the thymus and spleen (Fig. 3,4). Due to the presence of small but clear fractions of mature B and T cells in *Xlf*$^{-/-}$*Mri*$^{-/-}$*Trp53*$^{+/-}$ and *Xlf*$^{-/-}$*Paxx*$^{-/-}$*Trp53*$^{+/-}$ mice, we refer to the observed immunodeficient phenotypes as "leaky SCID". Previously, leaky SCID was described in mice lacking other NHEJ factors, e.g. *Ku70*$^{-/-}$ [5], *Artemis*$^{-/-}$ [7], *Lig4*$^{-/-}$*Trp53*$^{-/-}$, *Xrcc4*$^{-/-}$*Trp53*$^{-/-}$ [9, 29], *Xlf*$^{-/-}$*Atm*$^{-/-}$ [18] *and Xlf*$^{-/-}$*Rag2*$^{-/-}$ [21]. The Inactivation of *Trp53* is not always sufficient to rescue the embryonic lethality in mice. For example, the mice deficient for the PLK1-interacting checkpoint helicase (PICH) possess developmental defects in the presence or absence of p53 [31].

Moreover, we found that the mice with combined inactivation of *Paxx* and *Mri* (*Paxx*$^{-/-}$*Mri*$^{-/-}$) were live-born, fertile, and possessed normal B and T cell development. These data are further highlighting the previous observations using an *in vitro* model system. In particular, the vA*bl* pre-B cells with combined inactivation of *Paxx* and *Mri* genes showed as efficient V(D)J recombination as the single deficient *Mri*$^{-/-}$ and *Paxx*$^{-/-}$ and wild type controls [2]. Furthermore, combined inactivation of *Paxx* and *Ku80* (*Paxx*$^{-/-}$*Ku80*$^{-/-}$), *Atm* (*Paxx*$^{-/-}$*Atm*$^{-/-}$) [14], and *Dna-pkcs* (*Paxx*$^{-/-}$*Dna-pkcs*$^{-/-}$) [19] showed a similar phenotype to the single deficient mice, *Ku80*$^{-/-}$, *Atm*$^{-/-}$ and *Dna-pkcs*$^{-/-}$, correspondently. Thus, both *Paxx* and *Mri* interact genetically with *Xlf*, but not with each other or different DNA repair factors tested so far.

In conclusion, we have developed two complex genetic models, *Xlf*$^{-/-}$*Mri*$^{-/-}$*Trp53*$^{+/-}$ and *Xlf*$^{-/-}$ *Paxx*$^{-/-}$*Trp53*$^{+/-}$ and found that the B and T lymphocyte development is severely blocked in these mice at the progenitor stages.

Author contributions

All the authors designed the study, analyzed and interpreted the results. SCZ, QZ, and AL performed most of the experiments. VO wrote the paper with the help of SCZ and QZ.

Conflict of interest statement

The authors declare no conflict of interest.

Acknowledgments

This work was supported by the Research Council of Norway Young Talent Investigator grant (#249774) to V.O. In addition, VO's group was supported by the Liaison Committee for Education, Research, and Innovation in Central Norway (#13477; #38811); the Norwegian Cancer Society (#182355); the Research Council of Norway FRIMEDBIO grants (#270491 and #291217), and The Outstanding Academic Fellow Program at NTNU (2017–2021).

Figure legends

Fig. 1. Growth and immune system development in *Xlf$^{-/-}$Mri$^{-/-}$Trp53$^{+(-)/-}$* mice. (A) The comparison of body size, thymus and spleen size between a *Xlf$^{-/-}$Mri$^{-/-}$Trp53$^{+/-}$* mouse and an *Xlf$^{-/-}$* mouse of the same age. (B) The weight of WT, *Xlf$^{-/-}$*, *Mri$^{-/-}$*, *Xlf$^{-/-}$-Mri$^{-/-}$Trp53$^{+/-}$* mice. (C, D) The number ($\times 10^6$) of thymocytes (C) and splenocytes (D) in WT, *Xlf$^{-/-}$*, *Mri$^{-/-}$*, *Xlf$^{-/-}$-Mri$^{-/-}$Trp53$^{+/-}$* mice. Comparisons between every two groups were made using one-way ANOVA, GraphPad Prism 8.0.1. *XMT=*Xlf$^{-/-}$Mri$^{-/-}$Trp53$^{+/-}$*

Fig. 2. T and B cell development in *Xlf$^{-/-}$Mri$^{-/-}$Trp53$^{+/-}$* mice. (A) Flow cytometric analysis of thymic and splenic T cell subsets and splenic CD19+ B cells. (B; C; D) The number ($\times 10^6$) of splenic CD19+ B cells (B), splenic CD3+ T cells (C) and thymic CD4+CD8+ double positive (DP) T cells in WT, *Xlf$^{-/-}$*, *Mri$^{-/-}$*, *Xlf$^{-/-}$-Mri$^{-/-}$Trp53$^{+/-}$* mice. Comparisons between every two groups were made using one-way ANOVA, GraphPad Prism 8.0.1. *XMT=*Xlf$^{-/-}$Mri$^{-/-}$Trp53$^{+/-}$*; *XPT=*Xlf$^{-/-}$Paxx$^{-/-}$Trp53$^{+/-}$*; *DPK=*Dna-pkcs$^{-/-}$*

Fig. 3. T and B cell development in *Xlf*$^{-/-}$*Paxx*$^{-/-}$*Trp53*$^{+(-)/-}$ mice. Examples of flow cytometric analysis of thymic and splenic T cell subsets and splenic CD19+ B cells.

Fig. 4. B cell development is abrogated in bone marrow of *Xlf*$^{-/-}$*Mri*$^{-/-}$*Trp53*$^{+/-}$ and *Xlf*$^{-/-}$*Paxx*$^{-/-}$*Trp53*$^{+/-}$ mice. (A) Flow cytometric analysis of developing B cells. The upper left box marks progenitor B cell population, the lower left box marks the pre-B cells, and the lower right box marks the IgM+ immature and mature B cells. (B, C) The frequencies (%) of IgM+ B cells (B) and progenitor B cells (C) in WT, *Xlf*$^{-/-}$, *Mri*$^{-/-}$, *Xlf*$^{-/-}$*Mri*$^{-/-}$*Trp53*$^{+/-}$, *Paxx*$^{-/-}$, and *Xlf*$^{-/-}$*Paxx*$^{-/-}$*Trp53*$^{+/-}$ mice. Comparisons between every two groups were made using one-way ANOVA, GraphPad Prism 8.0.1. *XMT=*Xlf*$^{-/-}$*Mri*$^{-/-}$*Trp53*$^{+/-}$; *XPT=*Xlf*$^{-/-}$*Paxx*$^{-/-}$*Trp53*$^{+/-}$.

References

1. Kumar, V., F.W. Alt, and V. Oksenych, *Functional overlaps between XLF and the ATM-dependent DNA double strand break response.* DNA Repair (Amst), 2014. **16**: p. 11-22.
2. Hung, P.J., et al., *MRI Is a DNA Damage Response Adaptor during Classical Non-homologous End Joining.* Mol Cell, 2018. **71**(2): p. 332-342 e8.
3. Liu, X., et al., *PAXX promotes KU accumulation at DNA breaks and is essential for end-joining in XLF-deficient mice.* Nat Commun, 2017. **8**: p. 13816.
4. Gao, Y., et al., *A targeted DNA-PKcs-null mutation reveals DNA-PK-independent functions for KU in V(D)J recombination.* Immunity, 1998. **9**(3): p. 367-76.
5. Gu, Y., et al., *Growth retardation and leaky SCID phenotype of Ku70-deficient mice.* Immunity, 1997. **7**(5): p. 653-65.
6. Nussenzweig, A., et al., *Requirement for Ku80 in growth and immunoglobulin V(D)J recombination.* Nature, 1996. **382**(6591): p. 551-5.
7. Rooney, S., et al., *Leaky Scid phenotype associated with defective V(D)J coding end processing in Artemis-deficient mice.* Mol Cell, 2002. **10**(6): p. 1379-90.
8. Ma, Y., et al., *Hairpin opening and overhang processing by an Artemis/DNA-dependent protein kinase complex in nonhomologous end joining and V(D)J recombination.* Cell, 2002. **108**(6): p. 781-94.
9. Gao, Y., et al., *A critical role for DNA end-joining proteins in both lymphogenesis and neurogenesis.* Cell, 1998. **95**(7): p. 891-902.
10. Frank, K.M., et al., *Late embryonic lethality and impaired V(D)J recombination in mice lacking DNA ligase IV.* Nature, 1998. **396**(6707): p. 173-7.
11. Li, G., et al., *Lymphocyte-specific compensation for XLF/cernunnos end-joining functions in V(D)J recombination.* Mol Cell, 2008. **31**(5): p. 631-40.
12. Vera, G., et al., *Cernunnos deficiency reduces thymocyte life span and alters the T cell repertoire in mice and humans.* Mol Cell Biol, 2013. **33**(4): p. 701-11.
13. Abramowski, V., et al., *PAXX and Xlf interplay revealed by impaired CNS development and immunodeficiency of double KO mice.* Cell Death Differ, 2018. **25**(2): p. 444-452.
14. Balmus, G., et al., *Synthetic lethality between PAXX and XLF in mammalian development.* Genes Dev, 2016. **30**(19): p. 2152-2157.

15. Gago-Fuentes, R., et al., *Normal development of mice lacking PAXX, the paralogue of XRCC4 and XLF.* FEBS Open Bio, 2018. **8**(3): p. 426-434.
16. Liu, X., et al., *Overlapping functions between XLF repair protein and 53BP1 DNA damage response factor in end joining and lymphocyte development.* Proc Natl Acad Sci U S A, 2012. **109**(10): p. 3903-8.
17. Castaneda-Zegarra, S., et al., *Generation of a Mouse Model Lacking the Non-Homologous End-Joining Factor Mri/Cyren.* Biomolecules, 2019. **9**(12).
18. Zha, S., et al., *ATM damage response and XLF repair factor are functionally redundant in joining DNA breaks.* Nature, 2011. **469**(7329): p. 250-4.
19. Castaneda-Zegarra, S., et al., *Synthetic lethality between DNA repair factors Xlf and Paxx is rescued by inactivation of Trp53.* DNA Repair (Amst), 2019. **73**: p. 164-169.
20. Oksenych, V., et al., *Functional redundancy between repair factor XLF and damage response mediator 53BP1 in V(D)J recombination and DNA repair.* Proc Natl Acad Sci U S A, 2012. **109**(7): p. 2455-60.
21. Lescale, C., et al., *RAG2 and XLF/Cernunnos interplay reveals a novel role for the RAG complex in DNA repair.* Nat Commun, 2016. **7**: p. 10529.
22. Oksenych, V., et al., *Functional redundancy between the XLF and DNA-PKcs DNA repair factors in V(D)J recombination and nonhomologous DNA end joining.* Proc Natl Acad Sci U S A, 2013. **110**(6): p. 2234-9.
23. Xing, M., et al., *Synthetic lethality between murine DNA repair factors XLF and DNA-PKcs is rescued by inactivation of Ku70.* DNA Repair (Amst), 2017. **57**: p. 133-138.
24. Lescale, C., et al., *Specific Roles of XRCC4 Paralogs PAXX and XLF during V(D)J Recombination.* Cell Rep, 2016. **16**(11): p. 2967-2979.
25. Kumar, V., F.W. Alt, and R.L. Frock, *PAXX and XLF DNA repair factors are functionally redundant in joining DNA breaks in a G1-arrested progenitor B-cell line.* Proc Natl Acad Sci U S A, 2016. **113**(38): p. 10619-24.
26. Hung, P.J., et al., *Deficiency of XLF and PAXX prevents DNA double-strand break repair by non-homologous end joining in lymphocytes.* Cell Cycle, 2017. **16**(3): p. 286-295.
27. Jacks, T., et al., *Tumor spectrum analysis in p53-mutant mice.* Curr Biol, 1994. **4**(1): p. 1-7.
28. Castaneda-Zegarra, S., et al., *Generation of a Mouse Model Lacking the Non-Homologous End-Joining Factor Mri/Cyren. Biomolecules*, 2019. **9**(798).
29. Gao, Y., et al., *Interplay of p53 and DNA-repair protein XRCC4 in tumorigenesis, genomic stability and development.* Nature, 2000. **404**(6780): p. 897-900.
30. Frank, K.M., et al., *DNA ligase IV deficiency in mice leads to defective neurogenesis and embryonic lethality via the p53 pathway.* Mol Cell, 2000. **5**(6): p. 993-1002.
31. Albers, E., et al., *Loss of PICH Results in Chromosomal Instability, p53 Activation, and Embryonic Lethality.* Cell Rep, 2018. **24**(12): p. 3274-3284.

Figure 1

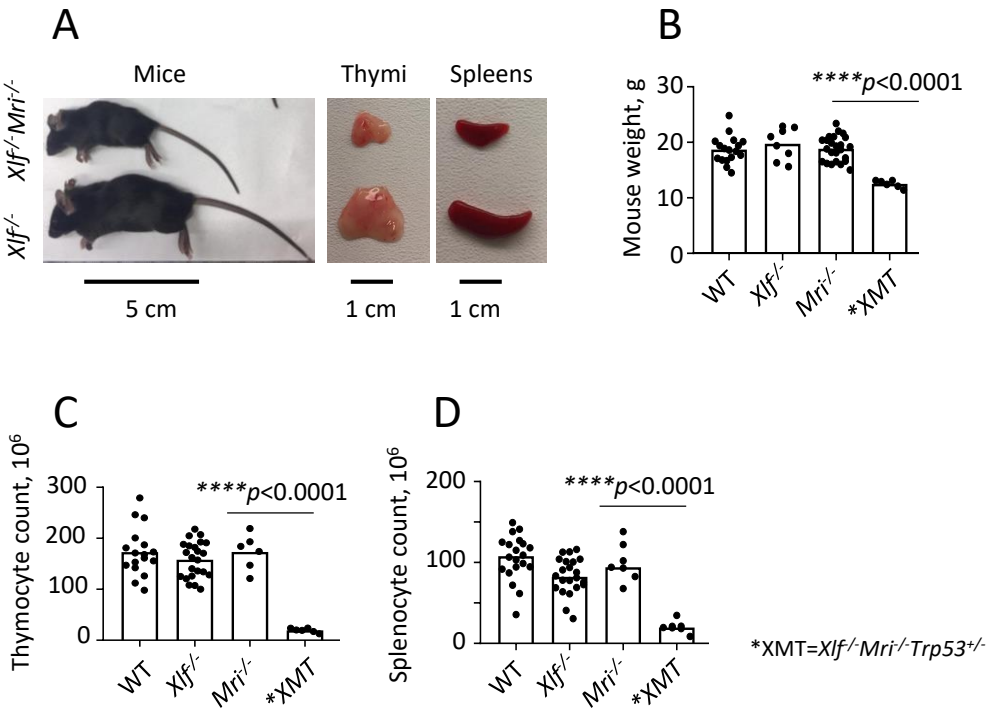
A
Mice
Thymi
Spleens
Xlf-/- Mri-/-
Xlf-/-
5 cm
1 cm
1 cm
B
Mouse weight, g
****p<0.0001
WT
Xlf-/-
Mri-/-
*XMT
C
Thymocyte count, 10^6
****p<0.0001
D
Splenocyte count, 10^6
****p<0.0001
*XMT=Xlf-/-Mri-/-Trp53+/-

Figure 2

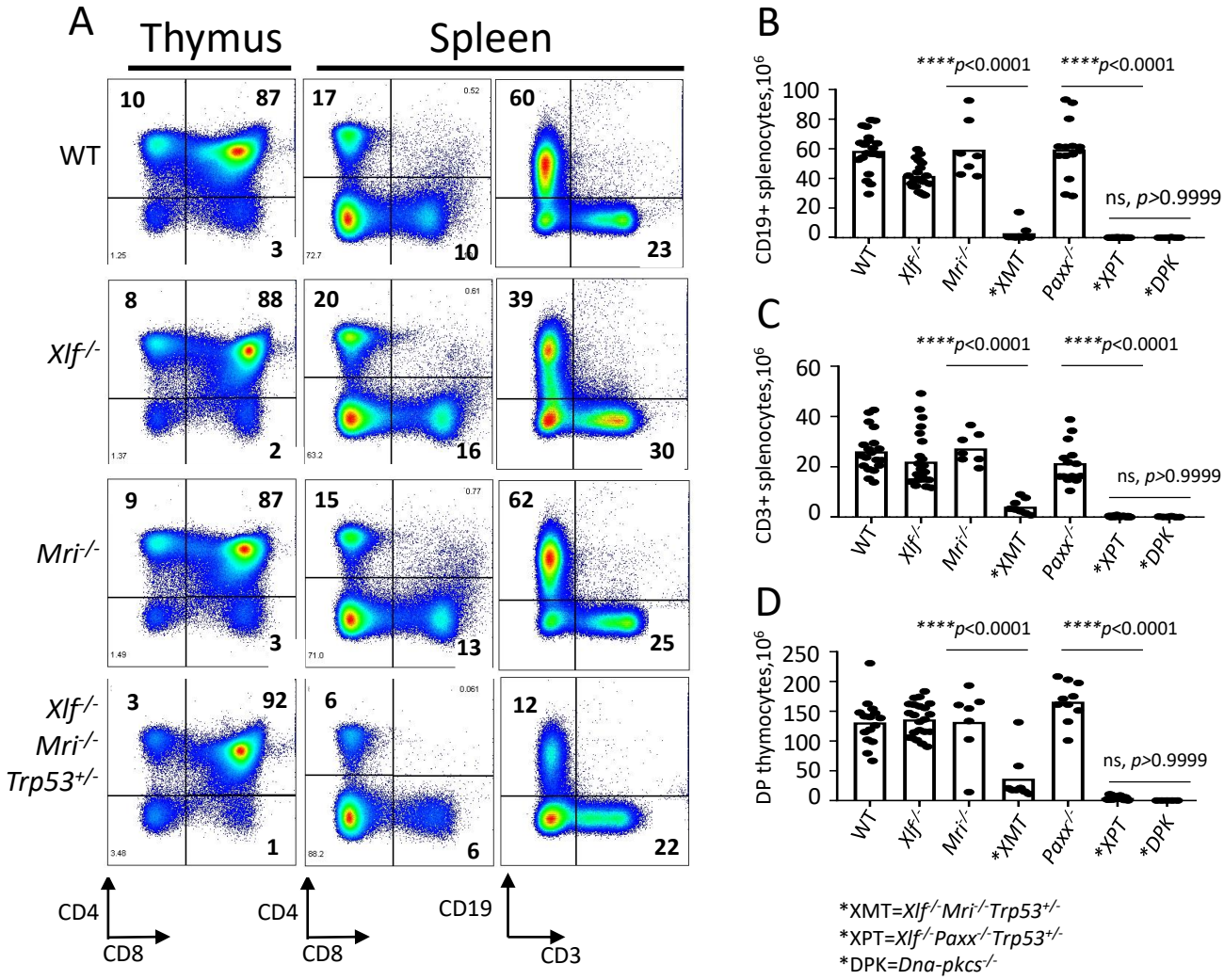
A
Thymus
Spleen
WT
Xlf-/-
Mri-/-
Xlf-/- Mri-/- Trp53+/-
10
87
3
17
60
10
23
8
88
2
20
39
16
30
9
87
3
15
62
13
25
3
92
1
6
12
6
22
CD4
CD8
CD4
CD8
CD19
CD3
B
CD19+ splenocytes,10^6
****p<0.0001
****p<0.0001
ns, p>0.9999
WT
Xlf-/-
Mri-/-
*XMT
Paxx-/-
*XPT
*DPK
C
CD3+ splenocytes,10^6
****p<0.0001
****p<0.0001
ns, p>0.9999
D
DP thymocytes,10^6
****p<0.0001
****p<0.0001
ns, p>0.9999
*XMT=Xlf-/-Mri-/-Trp53+/-
*XPT=Xlf-/-Paxx-/-Trp53+/-
*DPK=Dna-pkcs-/-

Figure 3

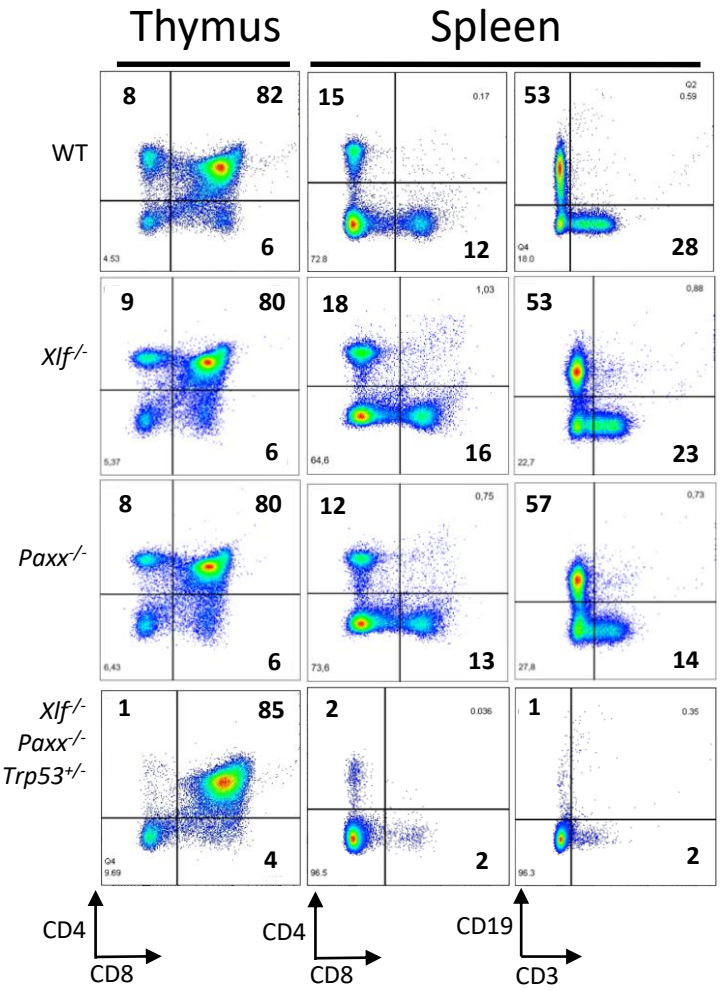
Thymus
Spleen
WT
Xlf-/-
Paxx-/-
Xlf-/-
Paxx-/-
Trp53+/-
8
82
6
15
12
53
28
9
80
6
18
16
53
23
8
80
6
12
13
57
14
1
85
4
2
2
1
2
CD4
CD8
CD4
CD8
CD19
CD3

Figure 4

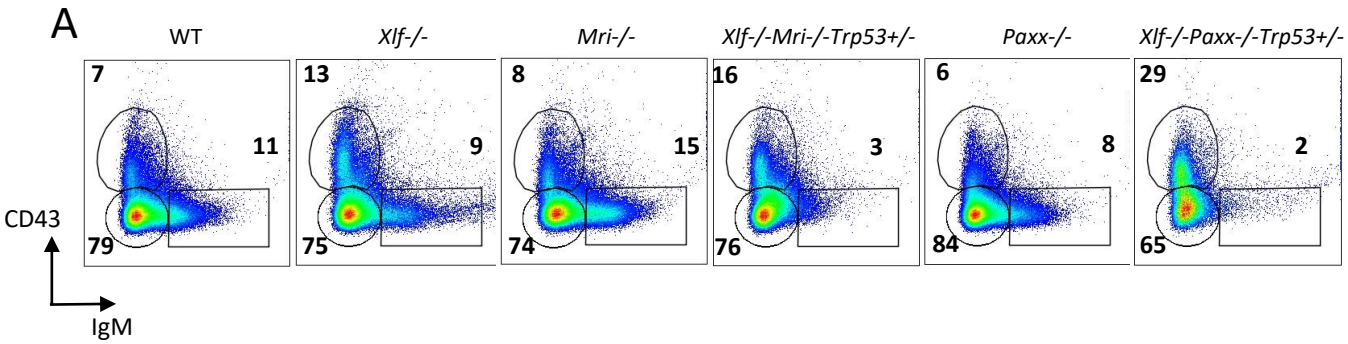

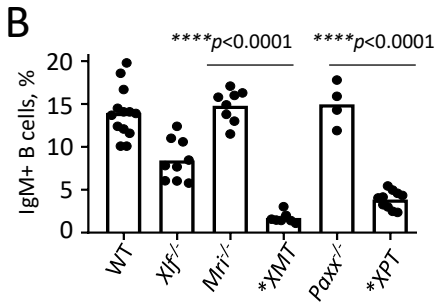

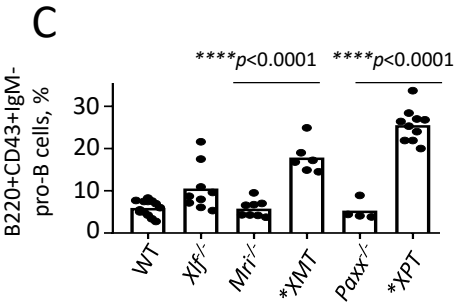

*XMT=*Xlf*$^{-/-}$*Mri*$^{-/-}$*Trp53*$^{+/-}$
*XPT=*Xlf*$^{-/-}$*Paxx*$^{-/-}$*Trp53*$^{+/-}$